

# High-pressure Mg-Sc-H phase diagram and its superconductivity from first-principles calculations

Peng Song,<sup>1</sup> Zhufeng Hou,<sup>2</sup> Pedro Baptista de Castro,<sup>3,4</sup> Kousuke Nakano,<sup>1,5</sup> Kenta Hongo,<sup>6</sup> Yoshihiko Takano,<sup>3,4</sup> and Ryo Maezono<sup>1</sup>

<sup>1</sup>*School of Information Science, JAIST, Asahidai 1-1, Nomi, Ishikawa 923-1292, Japan*

<sup>2</sup>*State Key Laboratory of Structural Chemistry, Fujian Institute of Research on the Structure of Matter, Chinese Academy of Sciences, Fuzhou 350002, China*

<sup>3</sup>*National Institute for Materials Science, 1-2-1 Sengen, Tsukuba, Ibaraki 305-0047, Japan*

<sup>4</sup>*University of Tsukuba, 1-1-1 Tennodai, Tsukuba, Ibaraki 305-8577, Japan*

<sup>5</sup>*International School for Advanced Studies (SISSA), Via Bonomea 265, 34136, Trieste, Italy*

<sup>6</sup>*Research Center for Advanced Computing Infrastructure, JAIST, Asahidai 1-1, Nomi, Ishikawa 923-1292, Japan*

(Dated: January 3, 2022)

In this work, global search for crystal structures of ternary Mg-Sc-H hydrides ( $\text{Mg}_x\text{Sc}_y\text{H}_z$ ) under high pressure ( $100 \leq P \leq 200$  GPa) were performed using the evolutionary algorithm and first-principles calculations. Based on them, we computed the thermodynamic convex hull and pressure-dependent phase diagram of  $\text{Mg}_x\text{Sc}_y\text{H}_z$  for  $z/(x+y) < 4$ . We have identified the stable crystal structures of four thermodynamically stable compounds with the higher hydrogen content, i.e.,  $R\bar{3}m\text{-MgScH}_6$ ,  $C2/m\text{-Mg}_2\text{ScH}_{10}$ ,  $Immm\text{-MgSc}_2\text{H}_9$  and  $Pm\bar{3}m\text{-Mg}(\text{ScH}_4)_3$ . Their superconducting transition temperatures were computationally predicted by the McMillan-Allen-Dynes formula combined with first-principles phonon calculations. They were found to exhibit superconductivity; among them,  $R\bar{3}m\text{-MgScH}_6$  was predicted to have the highest  $T_c$  (i.e. 23.34 K) at 200 GPa.

## I. INTRODUCTION

Hydrogen-rich hydrides of rare earth metals and alkaline earth metals are now recognized to be viable routes to realize room temperature superconductivity under high pressure. [1–4] These hydrides are usually stabilized with the clathrates consisting of H atoms, which could significantly lower the pressure-volume ( $PV$ ) term of enthalpy and thus preserve the stability at low pressures. [1, 5–12] In these structures, the H atoms can substantially contribute to the electronic density of states around the Fermi level and also the phonon density of states. Such a feature enables them to be the potential candidates to exhibit high-temperature superconductivity. For instance, theoretical calculations recently have predicted that  $\text{YH}_{10}$  with  $\text{H}_{32}$  cage structure might exhibit room-temperature superconductivity (286–326 K). [11]

For binary alkaline earth and rare earth hydrides, a systematic search for their crystal structures and superconductivity has been accomplished mostly by theoretical prediction, with the exception of few magnetic rare earth hydrides. [4, 13] The binary hydrides potentially with high-temperature superconductivity have attracted great attention for the experimental verification.  $\text{LaH}_{10}$ ,  $\text{CaH}_6$ ,  $\text{YH}_6$ ,  $\text{BaH}_{12}$  and  $\text{CeH}_9$  are the examples of the superconducting clathrate structures confirmed in experiments. [8, 14–17] The agreement between the theoretical prediction and the experimental discovery in the superconductivity of these binary hydrides has greatly encouraged the theoretical search for metal hydrides in a more extensive range such as the ternary case.

For ternary cases, a very recent experiment on the La-Y-H system has revealed that the synthesized  $(\text{La,Y})\text{H}_{10}$  at  $P = 180$  GPa exhibits a  $T_c$  of 253 K. [18] More interestingly, the pressure required for  $(\text{La,Y})\text{H}_{10}$  to achieve superconductivity is lower than that of  $\text{LaH}_{10}$  high-temperature superconductor, indicating that the ternary hydride has more potential in

the search for low-pressure room-temperature superconductivity. [11, 14]

The stability analysis and superconductivity prediction for a minor portion of ternary metal hydrides, such as La-Y-H, Ca-Y-H, Sc-Ca-H, Sc-Y-H, Y-Mg-H, and Ca-Mg-H, have been accomplished recently by theoretical calculations. [18–24] The majority of the high-temperature superconducting compounds in the aforementioned systems prefer to the cage-like structures. For example,  $Fd\bar{3}m\text{-CaYH}_{12}$  with cubic structure, preserves the clathrate structure consisting of the  $\text{H}_{24}$  cages, as does  $\text{CaH}_6$  and  $\text{YH}_6$ . Meanwhile  $Fd\bar{3}m\text{-CaYH}_{12}$  can remain stable above 170 GPa with a  $T_c$  value of 254 K as compared to  $\text{CaH}_6$  and  $\text{YH}_6$ . [1, 5, 20] Theoretical calculations further revealed that the strong electron-phonon coupling (EPC) in these clathrate structures of ternary metal hydrides is associated strongly to the phonon mode of the H-H bond in the cage. [20] Furthermore, the characteristics of these materials look very similar, including the atomic radius, electron number (spd valence electrons), electron negative, atomic mass of constituent elements and so on. [4] This might prevent the H cage from collapsing and preserve the same cage structure and superconductivity in the ternary hydride with clathrate structure.  $\text{ScCaH}_8$  and  $\text{ScCaH}_{12}$  are two potential high-temperature superconductor compounds in the Sc-Ca-H system. The cage structure is preserved in these two compounds and the corresponding  $T_c$  values are around 212 K and 182 K at 200 GPa, respectively. [21]

Motivated by the aforementioned studies, herein we concentrated our studies on the Mg-Sc-H system to explore the phase diagram and superconductivity of the associated ternary compounds under high pressure. By employing the evolutionary algorithm for crystal structure prediction, we have found the stable structures of  $\text{MgScH}_6$ ,  $\text{Mg}_2\text{ScH}_{10}$ ,  $\text{MgSc}_2\text{H}_9$ , and  $\text{Mg}(\text{ScH}_4)_3$  under high pressure, which are expected to have the highest hydrogen content in the ternary Mg-Sc-H com-

pounds. In the studied pressure range (i.e., 100-200 GPa), no stable compounds beyond the hydrogen content in the aforementioned compounds were discovered in the hydrogen-rich cases of Mg-Sc-H system, unlike the La-Y-H, Ca-Y-H, and other ternary systems. [18–24] Although some of the stable structures of ternary Mg-Sc-H compounds are predicted to exhibit superconductivity, their superconducting transition temperatures are high up to only 23.34 K at 200 GPa, owing to the relatively low density of states at their Fermi level and also a relatively weak electron-phonon coupling (EPC).

## II. METHOD

We considered the fixed compositions of ternary Mg-Sc-H compounds ( $\text{MgSc}_3\text{H}_x$ ,  $\text{MgSc}_2\text{H}_x$ ,  $\text{MgScH}_x$ ,  $\text{Mg}_2\text{ScH}_x$ , and  $\text{Mg}_3\text{ScH}_x$ , where  $x = 2-12, 14, 16$ , and  $18$ ) along selected lines in ternary convex hull at fixed pressure of 100 and 200 GPa. The crystal-structure search for the Mg-Sc-H systems was performed using the evolutionary algorithm implemented in the USPEX (Universal Structure Predictor: Evolutionary Xtallography) [25] software, together with the first-principles calculations of structural optimization based on density functional theory (DFT).

Our DFT structural optimization was carried out using the VASP (Vienna *ab initio* simulation package) [26–29] code. The electron-ion interaction is described by the projector augmented wave (PAW) [30, 31] method. The cutoff energy for plane-wave basis sets was set to 600 eV. The exchange and correlation potential was treated by the Perdew-Burke-Ernzerhof (PBE) functional [32] within generalized gradient approximation (GGA).

We computed the ternary convex hull of Mg-Sc-H system using the ConvexHull module in *scipy*, which involves evaluating Gibbs free energies of the predicted crystal structures at a finite temperature. [33] Their computational details are given in Supplemental Material (SM). The stable ternary phase was determined by a criteria that its enthalpy of formation should be smaller than the whole convex hull plane, which means such a phase would not decompose into any combination of elementary, binary, or other ternary phases.

The EPC and phonons of the stable ternary Mg-Sc-H phases were predicted using the QUANTUM ESPRESSO (QE) suite of programs [34–36] with the PAW method and the Perdew-Burke-Ernzerhof (PBE) [32] exchange correlation function. The cutoff energy for plane-wave basis sets in the QE calculations was set to 80 Ry. The  $k$  (and  $q$ )-point sampling for Broullion zone integration was set as follows:  $4 \times 4 \times 4$  ( $16 \times 16 \times 16$ ) for  $\text{MgScH}_6$ ,  $5 \times 5 \times 2$  ( $20 \times 20 \times 8$ ) for  $\text{Mg}_2\text{ScH}_{10}$ ,  $3 \times 4 \times 4$  ( $12 \times 16 \times 16$ ) for  $\text{MgSc}_2\text{H}_9$ ,  $5 \times 5 \times 5$  ( $20 \times 20 \times 20$ ) for  $\text{Mg}(\text{ScH}_4)_3$ , respectively. The McMillan-Allen-Dynes formula [37] and the Eliashberg function derived from the EPC calculation were used to predict the superconducting critical temperature.

## III. RESULTS AND DISCUSSION

### A. First-principles phase diagram of Mg-Sc-H system

To determine the ternary phase diagram of Mg-Sc-H system under high pressure, we have taken the Mg-H and Sc-H binary systems [1, 6, 9, 10, 38] as well as the simple substances of constituent elements (Mg, Sc, and H) [39–41] as references in the estimation of thermodynamic stability. It is worth noting that the superconducting structures of the Mg-H and Sc-H binary hydride systems have been discovered recently. For instance,  $\text{MgH}_6$  and  $\text{ScH}_7$  have been predicted to exhibit the highest  $T_c$  values of around 260 K and 169 K in the Mg-H and Sc-H binary system, respectively. [1, 6, 9, 10, 38] However, the pressure to stabilize these two superconducting compounds are both greater than 300 GPa, which is far beyond the mostly focused high-pressure range (i.e., around 200 GPa) of the widely studied metal hydrides in literature. [1, 5, 20, 42]

To explore the most likely composition for the succeeding experimental synthesis, herein we have sampled a wide phase space of the ternary Mg-Sc-H system at fixed pressures (i.e., 100 GPa and 200 GPa). The ternary phase diagram of the Mg-Sc-H system at 200 GPa is shown in Figure 1, while the results for the pressure at 100 GPa and the associated formation energies are given in the SM. Since most high-pressure studies are carried out under laser heating (1000-2000 K), some metastable phases at 0 K can be stabilized at higher temperatures. [18, 43] Therefore, herein we calculate the ternary phase diagram of Mg-Sc-H system at 200 GPa mainly in three different cases: i) formation enthalpy without considering the zero point energy (ZPE), ii) formation enthalpy with the contribution of ZPE and without the contribution of entropy, and iii) Gibbs free energy with the corresponding entropy contribution at 1000 K.

The stable compounds in the ternary convex hull of Mg-Sc-H system without ZPE at 200 GPa are  $Pm\bar{3}m\text{-Mg}_3\text{ScH}_3$ ,  $Pm\bar{3}m\text{-Mg}_3\text{ScH}_4$ ,  $C2/m\text{-Mg}_2\text{ScH}_{10}$ ,  $I4_1/amd\text{-MgScH}_2$ ,  $P6_3/mmc\text{-MgScH}_3$ ,  $P\bar{6}m2\text{-MgScH}_4$ ,  $R\bar{3}m\text{-MgScH}_6$ ,  $Immm\text{-MgSc}_2\text{H}_3$ ,  $R\bar{3}m\text{-Mg}(\text{ScH}_2)_2$ ,  $P6_3/mmc\text{-Mg}(\text{ScH}_2)_3$ ,  $Immm\text{-MgSc}_2\text{H}_9$  and  $Pm\bar{3}m\text{-Mg}(\text{ScH}_4)_3$ . It is noted that the incorporation of the ZPE contribution leads to the transition of  $\text{ScH}_4$  from a metastable state to a stable one, which is consistent with the results published by Ye et al. [9] for the binary Sc-H system.

On the other hand,  $Pm\bar{3}m\text{-Mg}_3\text{ScH}_4$ ,  $P6_3/mmc\text{-MgScH}_3$ ,  $R\bar{3}m\text{-MgScH}_6$ , and  $R\bar{3}m\text{-Mg}(\text{ScH}_2)_2$  undergo a change from a stable state to a metastable state because of their large contribution of the ZPE. The four ternary compounds are now equal to the convex hull plane, with energy differences of 0.003, 0.032, 0.008 and 0.015 eV/atom, respectively. Furthermore, we noticed that at a high temperature of 1000 K,  $R\bar{3}m\text{-Mg}(\text{ScH}_2)_2$  can shift from a metastable state to a stable one due to the entropy contribution of lattice vibration. In the binary Mg-H and Sc-H systems,  $Cmcm\text{-MgH}_4$  and  $Cmcm\text{-ScH}_6$  are the stable compounds with the greatest H content in the pressure range of 100-200 GPa. [6, 9] Despite the fact

that most of the existing high-temperature superconducting hydrides are hydrogen-rich compounds, no stable compounds in the extremely hydrogen-rich case have been identified in the pressure range of 100–200 GPa we searched. The ternary diagram package contains the synthetic routes for these stable compounds, and the connections of the binary and unary systems can be used as prospective candidates for the experimental synthesis of the ternary system.

Based on the calculated formation of enthalpy without accounting for the ZPE contribution, we summarize the pressure-dependent phase stability of Mg-Sc-H system and present it in Figure 2. In particular, several phases including  $Pm\bar{3}m$ -Mg(ScH<sub>4</sub>)<sub>3</sub>,  $Immm$ -MgSc<sub>2</sub>H<sub>10</sub>,  $P\bar{6}m2$ -MgScH<sub>4</sub>, and  $P6_3/mmc$ -MgScH<sub>3</sub> can be stable in a wide pressure range from 100 GPa to 200 GPa. It is remarkably to note that the Mg-rich ternary Mg-Sc-H phases prefer to be stable in the pressure range toward 200 GPa, while the Sc-rich ones except  $R\bar{3}m$ -Mg(ScH<sub>2</sub>)<sub>2</sub> can also be stabilized at the pressure of 100 GPa.  $P6_3/mmc$ -Mg(ScH<sub>2</sub>)<sub>2</sub> can be stable only in the lower pressure range of 100–130 GPa. This trend might be associated with the pressure range of stabilized binary Mg-H and Sc-H hydride systems. At the low pressure, the number of possible stable compounds in the Sc-H system are more than that of the Mg-H system. [6, 9]

## B. Predicted superconductivity of Mg-Sc-H system

Previous studies on the alkali metals and alkaline earth hydrides have shown that the superconducting properties of these hydrides are strongly dependent on the hydrogen content and that the higher  $T_c$  is more likely to appear in the hydrogen-rich cases. [1, 4] Herein we pay more attention to  $R\bar{3}m$ -MgScH<sub>6</sub>,  $C2/m$ -Mg<sub>2</sub>ScH<sub>10</sub>,  $Immm$ -MgSc<sub>2</sub>H<sub>9</sub>, and  $Pm\bar{3}m$ -Mg(ScH<sub>4</sub>)<sub>3</sub> for their electronic structures and superconductivity because they contain very high hydrogen content.

The crystal structures and the electron localization function (ELF) of these aforementioned four compounds are shown in Figure 3.  $R\bar{3}m$ -MgScH<sub>6</sub> is stable above 150 GPa and has a hexagonal crystal structure, in which each Mg and Sc atom is surrounded by 14 H atoms. The shortest H-H bond length in this structure is about 1.587 Å and the corresponding ELF value at the H-H bond center is about 0.4, indicating a nearly metallic character. The ultra-short distance between atoms translates to a significant ELF value of around 0.7, indicating that the H-H bond in  $C2/m$ -Mg<sub>2</sub>ScH<sub>10</sub> exhibits a strong covalent character. In  $Immm$ -MgSc<sub>2</sub>H<sub>9</sub> and  $Pm\bar{3}m$ -Mg(ScH<sub>4</sub>)<sub>3</sub>, the shortest H-H bond lengths are 1.628 Å and 1.650 Å, respectively, and the corresponding ELF values at the H-H bond center are 0.3 and 0.1. However the H lattice sites exhibit much greater ELF values. Therefore, the chemical bonding in  $Immm$ -MgSc<sub>2</sub>H<sub>9</sub> and  $Pm\bar{3}m$ -Mg(ScH<sub>4</sub>)<sub>3</sub> is mostly ionic interaction. Furthermore,  $Pm\bar{3}m$ -Mg(ScH<sub>4</sub>)<sub>3</sub> can still form a clathrate structure, in which each Mg and Sc atom is surrounded by the H14 cages. This structure may be regarded as a structure created when the central Sc in  $Fm\bar{3}m$ -ScH<sub>3</sub> is

replaced by Mg.

We should point out that  $Fm\bar{3}m$ -ScH<sub>3</sub> does not exhibit superconductivity, as reported previously by Ye et al, [9]. Therefore, the partial substitution of Sc in  $Fm\bar{3}m$ -ScH<sub>3</sub> by Mg triggers the superconductivity in  $Pm\bar{3}m$ -Mg(ScH<sub>4</sub>)<sub>3</sub>.

Figure 4 shows the calculated electronic energy band structure and atom-projected electronic density of states (eDOS) of the aforementioned four structures of great interest. All of them at 200 GPa exhibit metallic feature. Among these four structures,  $R\bar{3}m$ -MgScH<sub>6</sub> has most robust density of states at the Fermi level ( $E_F$ ), while  $Pm\bar{3}m$ -MgSc<sub>3</sub>H<sub>12</sub> has least density of states at  $E_F$ . The dominated contributions to the density of states at  $E_F$  come from the Sc and H atoms, while the contribution from Mg atoms is negligible. The valence bands in all of these four structures are mainly ascribed to the strong hybridization between Sc and H atoms. At the  $E_F$  of  $R\bar{3}m$ -MgScH<sub>6</sub>, there are doubly degenerated bands with very flat feature along the  $\Gamma \rightarrow Z$  direction (i.e., parallel to the  $c$  axis of the hexagonal unit cell of  $R\bar{3}m$ -MgScH<sub>6</sub>). Such a feature of flat band would aid in the electron-phonon interaction. [44] This also lead to the highest  $T_c$  of  $R\bar{3}m$ -MgScH<sub>6</sub> among these four structures.

Figure 5 shows the phonon band structure, atom-decomposed phonon density of states (pDOS), and Eliashberg spectra of  $R\bar{3}m$ -MgScH<sub>6</sub>,  $C2/m$ -Mg<sub>2</sub>ScH<sub>10</sub>,  $Immm$ -MgSc<sub>2</sub>H<sub>9</sub>, and  $Pm\bar{3}m$ -Mg(ScH<sub>4</sub>)<sub>3</sub> at 200 GPa. At first, we can see that there are no imaginary phonons in all of these four structures and so they are dynamically stable. In addition, their phonons can be clearly grouped into three frequency regions. The low frequency region (i.e., below 20 THz) is dominantly ascribed to the vibration of Mg and Sc atoms because of their heavier atomic masses. The middle frequency region (i.e., centered around 40 THz) and the high frequency region (i.e., above 50 THz) are exclusively contributed by the vibration of H atom.

Table 1 lists  $T_c$  values and their related quantities. The estimated EPC constants ( $\lambda$ ) of these four structures follow the ordering of  $R\bar{3}m$ -MgScH<sub>6</sub> >  $C2/m$ -Mg<sub>2</sub>ScH<sub>10</sub> >  $Immm$ -MgSc<sub>2</sub>H<sub>9</sub> >  $Pm\bar{3}m$ -Mg(ScH<sub>4</sub>)<sub>3</sub>. Their  $T_c$  values exhibit the same ordering.  $R\bar{3}m$ -MgScH<sub>6</sub> is found to have the highest  $T_c$  (i.e., 23.3 K) among these four structures at 200 GPa. However, this superconducting temperature is much lower than the reported other metal hydrides with high hydrogen content such as LaH<sub>10</sub> and YH<sub>10</sub>. [1, 4] This is due to the fact that the contribution of hydrogen atoms to the electronic density of states at  $E_F$  of these four structure is too low and the overall EPC constant is also too small. The contribution of heavy atoms (Mg and Sc) to the overall EPC constant in the low frequency range is extremely small, accounting for only about 8%.

It is interesting to note that YH<sub>3</sub> and  $Fm\bar{3}m$ -ScH<sub>3</sub> have the same hydrogen content per metal atom with  $R\bar{3}m$ -MgScH<sub>6</sub>,  $Immm$ -MgSc<sub>2</sub>H<sub>9</sub>, and  $Pm\bar{3}m$ -Mg(ScH<sub>4</sub>)<sub>3</sub>. However, YH<sub>3</sub> has a strong EPC constant of 1.6 and a  $T_c$  value of around 40 K. [45] In contrast, the EPC constant of  $Fm\bar{3}m$ -ScH<sub>3</sub> is about 0.23 and it hardly leads to the superconductivity. [9] The EPC



constants of aforementioned four structures of Mg-Sc-H are in the range from 0.35 to 0.54, and thus their superconducting transition temperatures are lower than that of  $\text{YH}_3$ .

#### IV. CONCLUSION

In summary, we have employed the evolutionary algorithm in the USPEX code and the first-principles calculations to explore the ternary phase diagram of the Mg-Sc-H system under pressure from 100 to 200 GPa. Our calculations show that the Sc-rich ternary Mg-Sc-H compounds are favorable to be stable around 100 GPa, while the Mg-rich ones are more likely to be stable above 180 GPa. The ternary Mg-Sc-H hydrides with the hydrogen/metal ratio around three have been predicted to exhibit the superconductivity. In particular, the superconducting transition temperature of  $R\bar{3}m$ -MgScH<sub>6</sub> is around 23 K at 200 GPa. Although the superconducting transition temperature of  $Pm\bar{3}m$ -Mg(ScH<sub>4</sub>)<sub>3</sub> is relatively low, it can be stable in the low range of high pressure toward 100 GPa. Our results provide

useful information for the discovery of new low-pressure superconducting hydrides.

#### ACKNOWLEDGMENTS

The computations in this work have been performed using the facilities of Research Center for Advanced Computing Infrastructure (RCACI) at JAIST. K.H. is grateful for financial support from the HPCI System Research Project (Project ID: hp190169) and MEXT-KAKENHI (JP16H06439, JP17K17762, JP19K05029, and JP19H05169) and the Air Force Office of Scientific Research (Award Numbers: FA2386-20-1-4036). R.M. is grateful for financial supports from MEXT-KAKENHI (19H04692 and 16KK0097), FLAGSHIP2020 (project nos. hp1 90169 and hp190167 at K-computer), Toyota Motor Corporation, I-O DATA Foundation, the Air Force Office of Scientific Research (AFOSR-AOARD/FA2386-17-1-4049; FA2386-19-1-4015), and JSPS Bilateral Joint Projects (with India DST).

- 
- [1] F. Peng, Y. Sun, C. J. Pickard, R. J. Needs, Q. Wu, and Y. Ma, *Phys. Rev. Lett.* **119**, 107001 (2017).
  - [2] E. Zurek, *Comments Inorg. Chem.* **37**, 78 (2016).
  - [3] E. Zurek and T. Bi, *J. Chem. Phys.* **150**, 050901 (2019).
  - [4] D. V. Semenov, I. A. Kruglov, I. A. Savkin, A. G. Kvashnin, and A. R. Oganov, *Curr. Opin. Solid State Mater. Sci.* **24**, 100808 (2020).
  - [5] H. Wang, J. S. Tse, K. Tanaka, T. Iitaka, and Y. Ma, *Proc. Natl. Acad. Sci.* **109**, 6463 (2012).
  - [6] X. Feng, J. Zhang, G. Gao, H. Liu, and H. Wang, *RSC Adv.* **5**, 59292 (2015).
  - [7] J. Hooper, T. Terpstra, A. Shamp, and E. Zurek, *J. Phys. Chem. C* **118**, 6433 (2014).
  - [8] W. Chen, D. V. Semenov, A. G. Kvashnin, X. Huang, I. A. Kruglov, M. Galasso, H. Song, D. Duan, A. F. Goncharov, V. B. Prakapenka, A. R. Oganov, and T. Cui, *Nat. Commun.* **12**, 1 (2021).
  - [9] X. Ye, N. Zarifi, E. Zurek, R. Hoffmann, and N. W. Ashcroft, *J. Phys. Chem. C* **122**, 6298 (2018).
  - [10] S. Qian, X. Sheng, X. Yan, Y. Chen, and B. Song, *Phys. Rev. B* **96**, 094513 (2017).
  - [11] H. Liu, I. I. Naumov, R. Hoffmann, N. W. Ashcroft, and R. J. Hemley, *Proc. Natl. Acad. Sci. USA* **114**, 6990 (2017).
  - [12] I. A. Kruglov, D. V. Semenov, H. Song, R. Szczesniak, I. A. Wrona, R. Akashi, M. M. D. Esfahani, D. Duan, T. Cui, A. G. Kvashnin, and A. R. Oganov, *Phys. Rev. B* **101**, 024508 (2020).
  - [13] J. A. Flores-Livas, L. Boeri, A. Sanna, G. Profeta, R. Arita, and M. Eremets, *Phys. Rep.* **856**, 1 (2020).
  - [14] A. P. Drozdov, P. P. Kong, V. S. Minkov, S. P. Besedin, M. A. Kuzovnikov, S. Mozaffari, L. Balicas, F. F. Balakirev, D. E. Graf, V. B. Prakapenka, E. Greenberg, D. A. Knyazev, M. Tkacz, and M. I. Eremets, *Nature* **569**, 528 (2019).
  - [15] I. A. Troyan, D. V. Semenov, A. G. Kvashnin, A. V. Sadakov, O. A. Sobolevskiy, V. M. Pudalov, A. G. Ivanova, V. B. Prakapenka, E. Greenberg, A. G. Gavriluk, I. S. Lyubutin, V. V. Struzhkin, A. Bergara, I. Errea, R. Bianco, M. Calandra, F. Mauri, L. Monacelli, R. Akashi, and A. R. Oganov, *Adv. Mater.* **33**, 2006832 (2021).
  - [16] L. Ma, K. Wang, Y. Xie, X. Yang, Y. Wang, M. Zhou, H. Liu, G. Liu, H. Wang, and Y. Ma, *arXiv preprint arXiv:2103.16282* (2021).
  - [17] N. P. Salke, M. M. D. Esfahani, Y. Zhang, I. A. Kruglov, J. Zhou, Y. Wang, E. Greenberg, V. B. Prakapenka, J. Liu, A. R. Oganov, and J.-F. Lin, *Nat. Commun.* **10**, 1 (2019).
  - [18] D. V. Semenov, I. A. Troyan, A. G. Ivanova, A. G. Kvashnin, I. A. Kruglov, M. Hanfland, A. V. Sadakov, O. A. Sobolevskiy, K. S. Pervakov, I. S. Lyubutin, K. V. Glazyrin, N. Giordano, D. N. Karimov, A. L. Vasiliev, R. Akashi, V. M. Pudalov, and A. R. Oganov, *Mater. Today*, 1369 (2021).
  - [19] P. Song, Z. Hou, P. B. de Castro, K. Nakano, K. Hongo, Y. Takano, and R. Maezono, *arXiv preprint arXiv:2103.06690* (2021).
  - [20] X. Liang, A. Bergara, L. Wang, B. Wen, Z. Zhao, X.-F. Zhou, J. He, G. Gao, and Y. Tian, *Phys. Rev. B* **99**, 100505 (2019).
  - [21] L.-T. Shi, Y.-K. Wei, A.-K. Liang, R. Turnbull, C. Cheng, X.-R. Chen, and G.-F. Ji, *J. Mater. Chem. C* **9**, 7284 (2021).
  - [22] Y. K. Wei, L. Q. Jia, Y. Y. Fang, L. J. Wang, Z. X. Qian, J. N. Yuan, G. Selvaraj, G. F. Ji, and D. Q. Wei, *Int. J. Quantum Chem.* **121**, e26459 (2020).
  - [23] P. Song, Z. Hou, P. B. de Castro, K. Nakano, K. Hongo, Y. Takano, and R. Maezono, *arXiv preprint arXiv:2107.05498* (2021).
  - [24] W. Sukmas, P. Tsuppayaakorn-aek, U. Pinsook, and T. Bovornratanaraks, *J. Alloys Compd.* **849**, 156434 (2020).
  - [25] C. W. Glass, A. R. Oganov, and N. Hansen, *Comput. Phys. Commun.* **175**, 713 (2006).
  - [26] G. Kresse and J. Hafner, *Phys. Rev. B* **47**, 558 (1993).
  - [27] G. Kresse and J. Hafner, *Phys. Rev. B* **49**, 14251 (1994).
  - [28] G. Kresse and J. Furthmüller, *Comput. Mater. Sci.* **6**, 15 (1996).
  - [29] G. Kresse and J. Furthmüller, *Phys. Rev. B* **54**, 11169 (1996).
  - [30] P. E. Blöchl, *Phys. Rev. B* **50**, 17953 (1994).
  - [31] G. Kresse and D. Joubert, *Phys. Rev. B* **59**, 1758 (1999).
  - [32] J. P. Perdew, K. Burke, and M. Ernzerhof, *Phys. Rev. Lett.* **77**, 3865 (1996).
  - [33] P. Virtanen, R. Gommers, T. E. Oliphant, M. Haberland, T. Reddy, D. Cournapeau, E. Burovski, P. Peterson,



- W. Weckesser, J. Bright, S. J. van der Walt, M. Brett, J. Wilson, K. J. Millman, N. Mayorov, A. R. J. Nelson, E. Jones, R. Kern, E. Larson, C. J. Carey, İ. Polat, Y. Feng, E. W. Moore, J. VanderPlas, D. Laxalde, J. Perktold, R. Cimrman, I. Henriksen, E. A. Quintero, C. R. Harris, A. M. Archibald, A. H. Ribeiro, F. Pedregosa, and P. van Mulbregt, *Nature Methods* **17**, 352 (2020).
- [34] P. Giannozzi, S. Baroni, N. Bonini, M. Calandra, R. Car, C. Cavazzoni, D. Ceresoli, G. L. Chiarotti, M. Cococcioni, I. Dabo, A. D. Corso, S. de Gironcoli, S. Fabris, G. Fratesi, R. Gebauer, U. Gerstmann, C. Gougoussis, A. Kokalj, M. Lazzeri, L. Martin-Samos, N. Marzari, F. Mauri, R. Mazzarello, S. Paolini, A. Pasquarello, L. Paulatto, C. Sbraccia, S. Scandolo, G. Sclauzero, A. P. Seitsonen, A. Smogunov, P. Umari, and R. M. Wentzcovitch, *J. Phys.: Condens. Matter* **21**, 395502 (2009).
- [35] P. Giannozzi, O. Andreussi, T. Brumme, O. Bunau, M. B. Nardelli, M. Calandra, R. Car, C. Cavazzoni, D. Ceresoli, M. Cococcioni, N. Colonna, I. Carnimeo, A. D. Corso, S. de Gironcoli, P. Delugas, R. A. DiStasio, A. Ferretti, A. Floris, G. Fratesi, G. Fugallo, R. Gebauer, U. Gerstmann, F. Giustino, T. Gorni, J. Jia, M. Kawamura, H.-Y. Ko, A. Kokalj, E. Küçükbenli, M. Lazzeri, M. Marsili, N. Marzari, F. Mauri, N. L. Nguyen, H.-V. Nguyen, A. O. de-la Roza, L. Paulatto, S. Poncé, D. Rocca, R. Sabatini, B. Santra, M. Schlipf, A. P. Seitsonen, A. Smogunov, I. Timrov, T. Thonhauser, P. Umari, N. Vast, X. Wu, and S. Baroni, *J. Phys.: Condens. Matter* **29**, 465901 (2017).
- [36] P. Giannozzi, O. Baseggio, P. Bonfà, D. Brunato, R. Car, I. Carnimeo, C. Cavazzoni, S. de Gironcoli, P. Delugas, F. F. Ruffino, A. Ferretti, N. Marzari, I. Timrov, A. Urru, and S. Baroni, *J. Chem. Phys.* **152**, 154105 (2020).
- [37] W. L. McMillan, *Phys. Rev.* **167**, 331 (1968).
- [38] D. C. Lonie, J. Hooper, B. Altintas, and E. Zurek, *Phys. Rev. B* **87**, 054107 (2013).
- [39] Q. Liu, C. Fan, and R. Zhang, *J. Appl. Phys.* **105**, 123505 (2009).
- [40] Y. Akahama, H. Fujihisa, and H. Kawamura, *Phys. Rev. Lett.* **94**, 195503 (2005).
- [41] C. J. Pickard and R. J. Needs, *Nat. Phys.* **3**, 473 (2007).
- [42] M. Einaga, M. Sakata, T. Ishikawa, K. Shimizu, M. I. Erements, A. P. Drozdov, I. A. Troyan, N. Hirao, and Y. Ohishi, *Nat. Phys.* **12**, 835 (2016).
- [43] A. Jayaraman, *Rev. Sci. Instrum.* **57**, 1013 (1986).
- [44] A. Simon, *Angew. Chem., Int. Ed. Engl.* **36**, 1788 (1997).
- [45] D. Y. Kim, R. H. Scheicher, and R. Ahuja, *Phys. Rev. Lett.* **103**, 077002 (2009).
- [46] K. Momma and F. Izumi, *Journal of Applied Crystallography* **44**, 1272 (2011).

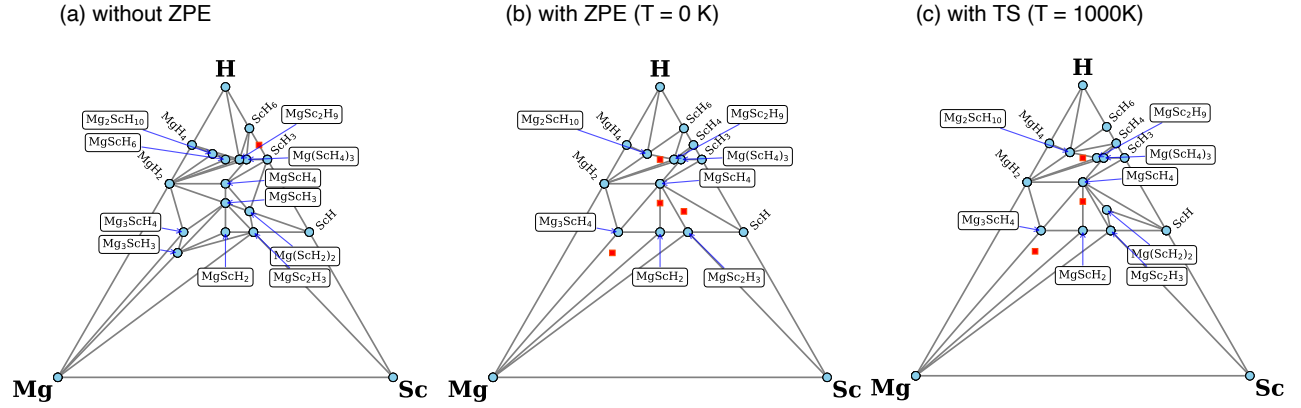


FIG. 1. Ternary convex hulls of the Mg-Sc-H system at a pressure of 200 GPa. (b), (c) are the convex hulls of Gibbs free energy at finite temperature. The stable and metastable phases are shown by blue circles and red squares, respectively.

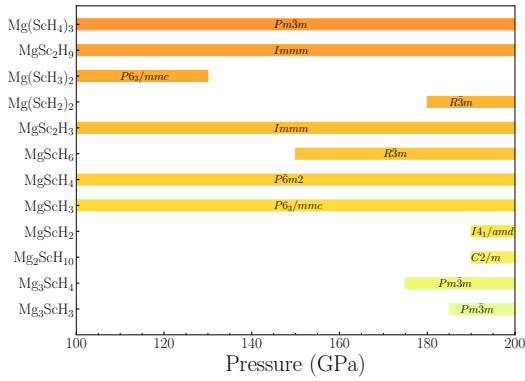


FIG. 2. Phase diagram of Mg-Sc-H in the pressure range of 100–200 GPa.

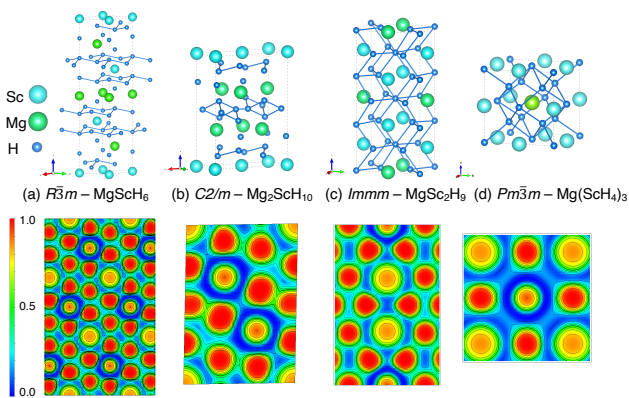


FIG. 3. Predicted crystal structures of (a)  $R\bar{3}m$ - $\text{MgScH}_6$ , (b)  $C2/m$ - $\text{Mg}_2\text{ScH}_{10}$ , (c)  $Immm$ - $\text{MgSc}_2\text{H}_9$ , (d)  $Pm\bar{3}m$ - $\text{Mg}(\text{ScH}_4)_3$  at 200 GPa. Bottom panels show the corresponding contour plots of electron localization function (ELF) in these structures. These structural models were drawn by using VESTA. [46]

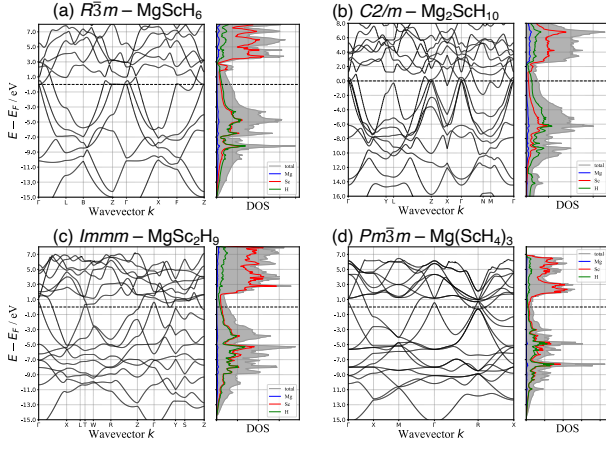


FIG. 4. Electronic band structures and atom-projected electronic density of states of (a)  $R\bar{3}m$ -MgScH<sub>6</sub>, (b)  $C2/m$ -Mg<sub>2</sub>ScH<sub>10</sub>, (c)  $Immm$ -MgSc<sub>2</sub>H<sub>9</sub>, (d)  $Pm\bar{3}m$ -Mg(ScH<sub>4</sub>)<sub>3</sub> at 200 GPa.

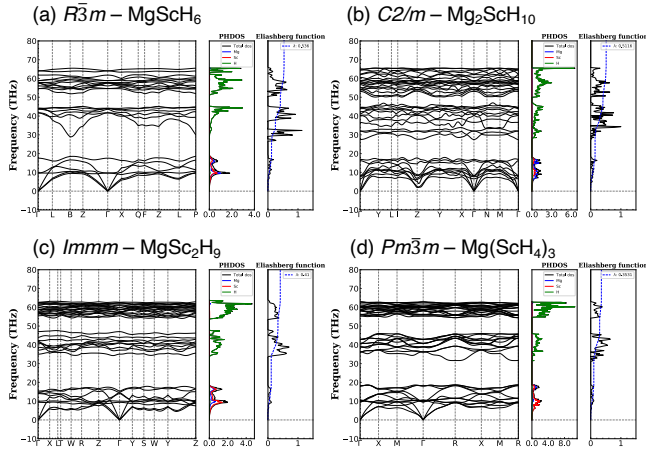


FIG. 5. Phonon dispersion and atom-projected phonon density of states (pDOS), and Eliashberg spectral of (a)  $R\bar{3}m$ -MgScH<sub>6</sub>, (b)  $C2/m$ -Mg<sub>2</sub>ScH<sub>10</sub>, (c)  $Immm$ -MgSc<sub>2</sub>H<sub>9</sub>, (d)  $Pm\bar{3}m$ -Mg(ScH<sub>4</sub>)<sub>3</sub> at 200 GPa.

TABLE I.  $T_c$  estimated by McMillan formula using first-principles phonon calculations for Mg-Sc-H at each pressure.  $\lambda$  and  $\omega_{\log}$  are the parameters appearing in the formula.

Phase	Space group	$P$ (GPa)	$\lambda$	$\omega_{\log}$ (K)	$N_{E_F}$ (states/eV/Å <sup>3</sup> ) at $\mu = 0.1 - 0.13$	$T_c$ (K)
MgScH <sub>6</sub>	$R\bar{3}/m$	200	0.536	1478.84	0.0150	23.34 – 15.08
Mg <sub>2</sub> ScH <sub>10</sub>	$C2/m$	200	0.512	1350.17	0.0125	17.94 – 11.10
MgSc <sub>2</sub> H <sub>9</sub>	$Immm$	200	0.410	1427.39	0.0120	6.88 – 3.14
MgSc <sub>3</sub> H <sub>12</sub>	$Pm\bar{3}m$	200	0.353	1377.73	0.0102	2.61 – 0.83



# Supplemental Material

for

## First-principles study on the phase diagram and superconductivity of Mg-Sc-H system under high pressure

Peng Song,<sup>1</sup> Zhufeng Hou,<sup>2</sup> Pedro Baptista de Castro,<sup>3,4</sup> Kousuke Nakano,<sup>1,5</sup> Kenta Hongo,<sup>6</sup> Yoshihiko Takano,<sup>3,4</sup> and Ryo Maezono<sup>1</sup>

<sup>1</sup>*School of Information Science, JAIST, Asahidai 1-1, Nomi, Ishikawa 923-1292, Japan*

<sup>2</sup>*State Key Laboratory of Structural Chemistry, Fujian Institute of Research on the Structure of Matter, Chinese Academy of Sciences, Fuzhou 350002, China*

<sup>3</sup>*National Institute for Materials Science, 1-2-1 Sengen, Tsukuba, Ibaraki 305-0047, Japan*

<sup>4</sup>*University of Tsukuba, 1-1-1 Tennodai, Tsukuba, Ibaraki 305-8577, Japan*

<sup>5</sup>*International School for Advanced Studies (SISSA), Via Bonomea 265, 34136, Trieste, Italy*

<sup>6</sup>*Research Center for Advanced Computing Infrastructure, JAIST, Asahidai 1-1, Nomi, Ishikawa 923-1292, Japan*

### A. Computational details

The Gibbs free energy of the chemical compounds in the Sc-Mg-H system was calculated according to the following equation:

$$G(T) = F(T) + pV, \quad (S1)$$

where  $F(T)$  is the Helmholtz free energy as defined below:

$$F(T) = U(T) - TS(T). \quad (S2)$$

The internal energy  $U(T)$  and entropy  $S(T)$  are given by the following equations:

$$U(T) = E_{\text{elec}} + \int_0^\infty \left[ \frac{\varepsilon}{e^{\frac{\varepsilon}{k_B T}} - 1} + \frac{\varepsilon}{2} \right] \sigma(\varepsilon) d\varepsilon, \quad (S3)$$

$$S(T) = \int_0^\infty \left[ \frac{\varepsilon}{T} \frac{1}{e^{\frac{\varepsilon}{k_B T}} - 1} - \kappa_B \ln(1 - e^{-\frac{\varepsilon}{k_B T}}) \right] \sigma(\varepsilon) d\varepsilon. \quad (S4)$$

Here  $\sigma(\varepsilon)$  represents the phonon density of states as a function of vibrational energy and is obtained by the lattice dynamics calculation using the Phonopy code.<sup>1</sup>  $E_{\text{elec}}$  is the electronic energy from the DFT calculations.

The superconducting critical temperature was predicted according to the McMillan-Allen-Dynes formula:<sup>2</sup>

$$T_c = \frac{\omega_{\log}}{1.2} \exp \left( \frac{-1.04(1 + \lambda)}{\lambda(1 - 0.62\mu^*) - \mu^*} \right), \quad (S5)$$

where  $\omega_{\log}$  and  $\lambda$  are the logarithmic average phonon frequency and electron-phonon coupling (EPC) constant obtained in the Eliashberg function.

## B. Supplementary figures

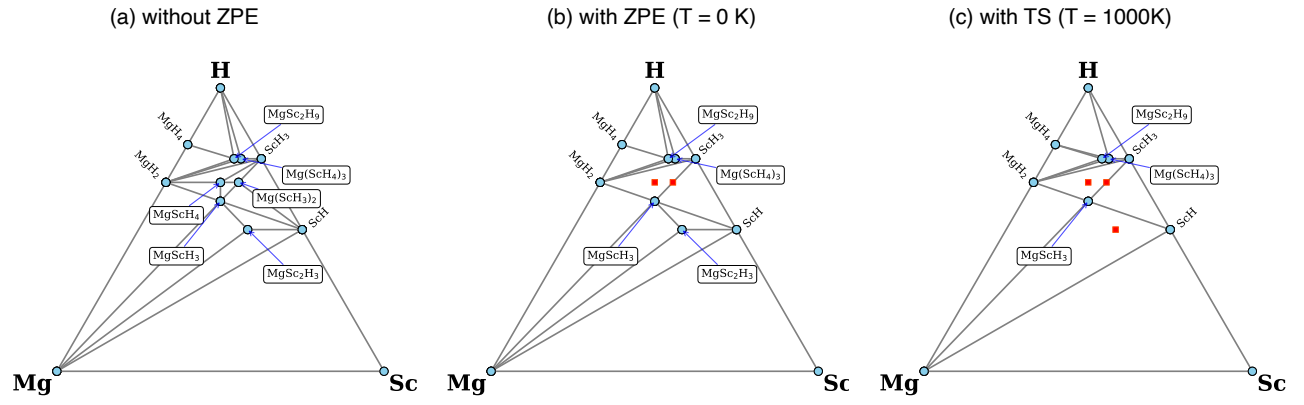


FIG. S1: Ternary convex hulls of the Mg-Sc-H system at a pressure of 100 GPa.

## C. Supplementary tables

TABLE S1: The Gibbs free energy and enthalpy value of Mg-Sc-H at 100GPa at a finite temperature. The metastable phase is shown by the red text in the figure, and the energy value above the convex hull is indicated by the number in brackets.

Formula	Space group	Nites	PV (eV/atom)	Enthalpy (eV/atom)	ZPE (eV/atom)	G (T = 0 K) (eV/atom)	G (T = 1000 K) (eV/atom)
Mg	<i>Im<math>\bar{3}m</math></i>	1	14.0401	7.57398	0.07276	7.64674	7.4084
Sc	<i>P6<sub>2</sub>22</i>	3	14.964	3.82559	0.03295	3.85854	3.55277
H	<i>C2/c</i>	12	2.8488	-1.20802	0.27219	-0.93583	-1.03683
MgH2	<i>P6<sub>3</sub>/mmc</i>	6	5.677	0.83324	0.21098	1.04422	0.94367
MgH4	<i>Cmcm</i>	10	4.4777	-0.02043	0.21336	0.19293	0.10469
ScH	<i>Fm<math>\bar{3}m</math></i>	2	8.7637	0.17971	0.16433	0.34405	0.14192
ScH3	<i>Fm<math>\bar{3}m</math></i>	4	5.5659	-1.24658	0.20921	-1.03737	-1.13512
MgScH3	<i>P6<sub>3</sub>/mmc</i>	10	7.0434	0.39592	0.18754	0.58346	0.46915
MgScH4	<i>P6m2</i>	6	6.1657	-0.07849	0.25699	0.1785 (+0.02)	0.06299 (+0.01)
MgSc2H3	<i>Immm</i>	6	8.3424	0.87244	0.16994	1.04238	0.89664(+0.013)
Mg(ScH3)2	<i>P6<sub>3</sub>/mmc</i>	18	6.3831	-0.33496	0.19989	-0.13507 (+0.002)	-0.24167 (+0.002)
MgSc2H9	<i>Immm</i>	12	5.3076	-0.77339	0.2173	-0.5561	-0.64476
Mg(ScH4)3	<i>Pm<math>\bar{3}m</math></i>	16	5.3679	-0.90105s	0.21949	-0.68156	-0.77673

TABLE S2: 200GPa

Formula	Space group	Nites	PV (eV/atom)	Enthalpy (eV/atom)	ZPE (eV/atom)	G (T = 0 K) (eV/atom)	G (T = 1000 K) (eV/atom)
Mg	<i>Im<math>\bar{3}m</math></i>	1	11.225	13.793	0.088	13.881	13.678
Sc	<i>C222</i>	3	11.385	10.272	0.042	10.314	10.062
H	<i>C2/c</i>	12	2.15	0.0182	0.293	0.311	0.2417
MgH2	<i>P6<sub>3</sub>/mmc</i>	6	4.598	3.372	0.267	3.639	3.562
MgH4	<i>Cmcm</i>	10	3.578	1.964	0.276	2.24	2.173
ScH	<i>Fm<math>\bar{3}m</math></i>	2	7.124	4.103	0.209	4.312	4.169
ScH3	<i>Fm<math>\bar{3}m</math></i>	4	4.654	1.282	0.258	1.540	1.457
ScH4	<i>I4/mmm</i>	5	3.956	1.022 (+0.007)	0.233	1.255	1.176
ScH6	<i>Cmcm</i>	14	3.462	0.711	0.263	0.974	0.907
Mg3ScH3	<i>Pm<math>\bar{3}m</math></i>	7	7.149	6.464	0.205	6.669	6.543 (+0.02)
Mg3ScH4	<i>Pm<math>\bar{3}m</math></i>	7	6.384	5.415	0.196	5.611 (+0.015)	5.491
Mg2ScH10	<i>C2/m</i>	13	3.999	1.888	0.261	2.149	2.074
MgScH2	<i>I4<sub>1</sub>/amd</i>	8	6.598	4.922	0.205	5.127	5.009
MgScH3	<i>P6<sub>3</sub>/mmc</i>	10	5.722	3.551	0.289	3.84 (+0.032)	3.743 (+0.036)
MgScH4	<i>P6m2</i>	6	5.069	2.7	0.229	2.928	3.743
MgScH6	<i>R<math>\bar{3}m</math></i>	8	4.295	1.843	0.228	2.118 (+0.008)	2.043 (+0.009)
MgSc2H3	<i>Immm</i>	6	6.764	4.602	0.22	4.822	4.699
Mg(ScH2)2	<i>R3m</i>	14	6.101	3.702	0.238	3.94 (+0.003)	3.823
MgSc2H9	<i>Immm</i>	12	4.406	1.629	0.268	1.897	1.821
Mg(ScH4)3	<i>Pm<math>\bar{3}m</math></i>	16	4.464	1.532	0.266	1.799	1.722

TABLE S3: Crystal structures of Mg-Sc-H predicted at each pressure (*P*). Lattice parameters (*a*, *b* and *c*) are given in unit of Å.

Compound	Space group	<i>P</i> (GPa)	Lattice parameters	Atomic coordinates (fractional)			
				Atoms	<i>x</i>	<i>y</i>	<i>z</i>
Mg <sub>3</sub> ScH <sub>3</sub>	<i>Pm<math>\bar{3}m</math></i>	200	$a = b = c = 3.8598$	Mg(3c)	0.00000	0.50000	0.50000
				Sc(1a)	0.00000	0.00000	0.00000
				H(3d)	0.00000	0.00000	0.50000
				$\alpha = \beta = \gamma = 90^\circ$			
Mg <sub>3</sub> ScH <sub>4</sub>	<i>Pm<math>\bar{3}m</math></i>	200	$a = b = c = 3.44577$	Mg(3d)	0.00000	0.00000	0.50000
				Sc(1b)	0.50000	0.50000	0.50000
				H(3c)	0.00000	0.50000	0.50000
				$\alpha = \beta = \gamma = 90^\circ$			

Continued on next page



TABLE S3 – continued from previous page

Compound	Space group	$P$ (GPa)	Lattice parameters	Atomic coordinates (fractional)			
				Atoms	$x$	$y$	$z$
				H(1a)	0.00000	0.00000	0.00000
Mg <sub>2</sub> ScH <sub>10</sub>	$C2/m$	200	$a = 4.68347$	Mg(4i)	0.14842	0.50000	0.66872
			$b = 2.66303$	Sc(2a)	0.00000	0.00000	0.00000
			$c = 6.68240$	H(4i)	0.01613	0.00000	0.25389
			$\alpha = \gamma = 90^\circ$	H(4i)	0.08363	0.00000	0.50129
			$\beta = 91.8666^\circ$	H(4i)	0.16487	0.50000	0.90258
				H(4i)	0.17516	0.50000	0.15337
				H(4i)	0.18058	0.50000	0.41760
MgScH <sub>2</sub>	$I4_1/amd$	200	$a = b = 3.44323$	Mg(4b)	0.00000	0.00000	0.50000
			$c = 7.13282$	Sc(4a)	0.00000	0.00000	0.00000
			$\alpha = \beta = \gamma = 90^\circ$	H(8e)	0.00000	0.00000	0.25034
MgScH <sub>3</sub>	$P6_3/mmc$	200	$a = b = 2.68846$	Mg(2c)	0.33333	0.66667	0.25000
			$c = 7.32296$	Sc(2a)	0.00000	0.00000	0.00000
			$\alpha = \beta = 90^\circ$	H(4f)	0.33333	0.66667	0.88193
			$\gamma = 120^\circ$	H(2b)	0.00000	0.00000	0.25000
MgScH <sub>4</sub>	$P\bar{6}m2$	200	$a = b = 2.81444$	Mg(1a)	0.00000	0.00000	0.00000
			$c = 3.55190$	Sc(1d)	0.33333	0.66667	0.50000
			$\alpha = \beta = 90^\circ$	H(2i)	0.66667	0.33333	0.25516
			$\gamma = 120^\circ$	H(1b)	0.00000	0.00000	0.50000
				H(1c)	0.33333	0.66667	0.00000
MgScH <sub>6</sub>	$R\bar{3}m$	200	$a = b = 2.66735$	Mg(3b)	-0.00000	-0.00000	0.50000
			$c = 13.40164$	Sc(3a)	0.00000	0.00000	0.00000
			$\alpha = \beta = 90^\circ$	H(6c)	0.00000	0.00000	0.12672
			$\gamma = 120^\circ$	H(6c)	0.00000	0.00000	0.25502
				H(6c)	0.00000	0.00000	0.38301
MgSc <sub>2</sub> H <sub>3</sub>	$Immm$	200	$a = 2.54852$	Mg(2b)	0.00000	0.50000	0.50000
			$b = 3.45765$	Sc(4j)	0.00000	0.50000	0.16137
			$c = 7.37865$	H(4i)	0.00000	0.00000	0.16481
			$\alpha = \beta = \gamma = 90^\circ$	H(2c)	0.00000	0.00000	0.50000
MgSc <sub>2</sub> H <sub>4</sub>	$R\bar{3}m$	300	$a = b = 2.57905$	Mg(6c)	0.00000	0.00000	0.19177
			$c = 35.63329$	Sc(6c)	0.00000	0.00000	0.08687
			$\alpha = \beta = 90^\circ$	Sc(6c)	0.00000	0.00000	0.36179
			$\gamma = 120^\circ$	H(6c)	0.00000	0.00000	0.13761
				H(6c)	0.00000	0.00000	0.27601
				H(6c)	0.00000	0.00000	0.44780
				H(3a)	-0.00000	-0.00000	0.50000
				H(3a)	0.00000	0.00000	0.00000
MgSc <sub>2</sub> H <sub>6</sub>	$P6_3/mmc$	100	$a = b = 2.92493$	Mg(2d)	0.33333	0.66667	0.75000
			$c = 12.42285$	Sc(4f)	0.33333	0.66667	0.40589
			$\alpha = \beta = 90^\circ$	H(4e)	0.00000	0.00000	0.16535
			$\gamma = 120^\circ$	H(4f)	0.33333	0.66667	0.55450
				H(2a)	0.00000	0.00000	0.00000
				H(2c)	0.33333	0.66667	0.25000
MgSc <sub>2</sub> H <sub>9</sub>	$Immm$	200	$a = 2.69052$	Mg(2d)	0.00000	0.50000	0.00000
			$b = 3.86680$	Sc(4j)	0.00000	0.50000	0.33646
			$c = 8.14298$	H(8l)	0.00000	0.26386	0.16221
			$\alpha = \beta = \gamma = 90^\circ$	H(4i)	0.00000	0.00000	0.32780
				H(4h)	0.00000	0.23179	0.50000
				H(2a)	0.00000	0.00000	0.00000
MgSc <sub>3</sub> H <sub>12</sub>	$Pm\bar{3}m$	200	$a = b = c = 3.85331$	Mg(1b)	0.50000	0.50000	0.50000
			$\alpha = \beta = \gamma = 90^\circ$	Sc(3d)	0.00000	0.00000	0.50000
				H(8g)	0.25894	0.25894	0.25894
				H(3c)	0.00000	0.50000	0.50000
				H(1a)	0.00000	0.00000	0.00000

- 
- <sup>1</sup> A. Togo and I. Tanaka, *Scripta Materialia* **108**, 1 (2015).  
<sup>2</sup> W. L. McMillan, *Phys. Rev.* **167**, 331 (1968).